Electronic Supplementary Information

Strategies for the Selective Loading of Patchy Worm-Like Micelles with Functional Nanoparticles

Judith Schöbel,[a] Christian Hils,[a] Anne Weckwerth,[b] Mathias Schlenk,[b] Carina Bojer,[c] Marc C. A. Stuart,[d] Josef Breu,[c,e] Stephan Förster,[b,†] Andreas Greiner,[a,e] Matthias Karg[b,‡] and Holger Schmalz[a,e*]

a) Makromolekulare Chemie II, Universität Bayreuth, 95440 Bayreuth, Germany

b) Physikalische Chemie I, Universität Bayreuth, 95440 Bayreuth, Germany

c) Anorganische Chemie I, Universität Bayreuth, 95440 Bayreuth, Germany

d) Stratingh Institute for Chemistry and Electron Microscopy, Group Groningen, Biomolecular Sciences and Biotechnology Institute, University of Groningen, 9747 AG Groningen, The Netherlands

e) Bavarian Polymer Institute (BPI), Universität Bayreuth, 95440 Bayreuth, Germany

†) present address: JCNS-1/ICS-1, Forschungszentrum Jülich, 52425 Jülich, Germany

‡) present address: Physikalische Chemie I, Heinrich-Heine-Universität Düsseldorf, 40204 Düsseldorf, Germany

1. Characterisation of ZnO and CuO NPs

The ZnO and CuO NPs were analysed by powder X-Ray diffraction to confirm the phase purity (Fig. S1A). For both types of NPs, the measured peaks can be clearly assigned to ZnO (PDF: 00-036-1451) and CuO (PDF: 45-0937), respectively. For CuO NPs only the two most intense peaks can be found as reported by Kida et. al.[1] The peaks of both NP types show a high full width at half maximum (FWHM), confirming the formation of NPs. Dynamic light scattering (DLS) reveals narrow particle size distributions (Fig. S1B) with average hydrodynamic diameters of 3.2 ± 0.1 nm for ZnO and 5.8 ± 1.4 nm for CuO NPs, respectively. From TEM image analysis (Fig. S1C, D) average diameters of 2.7 ± 0.4 nm for ZnO NPs and 3.8 ± 0.6 nm for CuO NPs were obtained. As expected, the sizes from DLS are slightly higher compared to that determined by TEM, as DLS probes the hydrodynamic diameters.

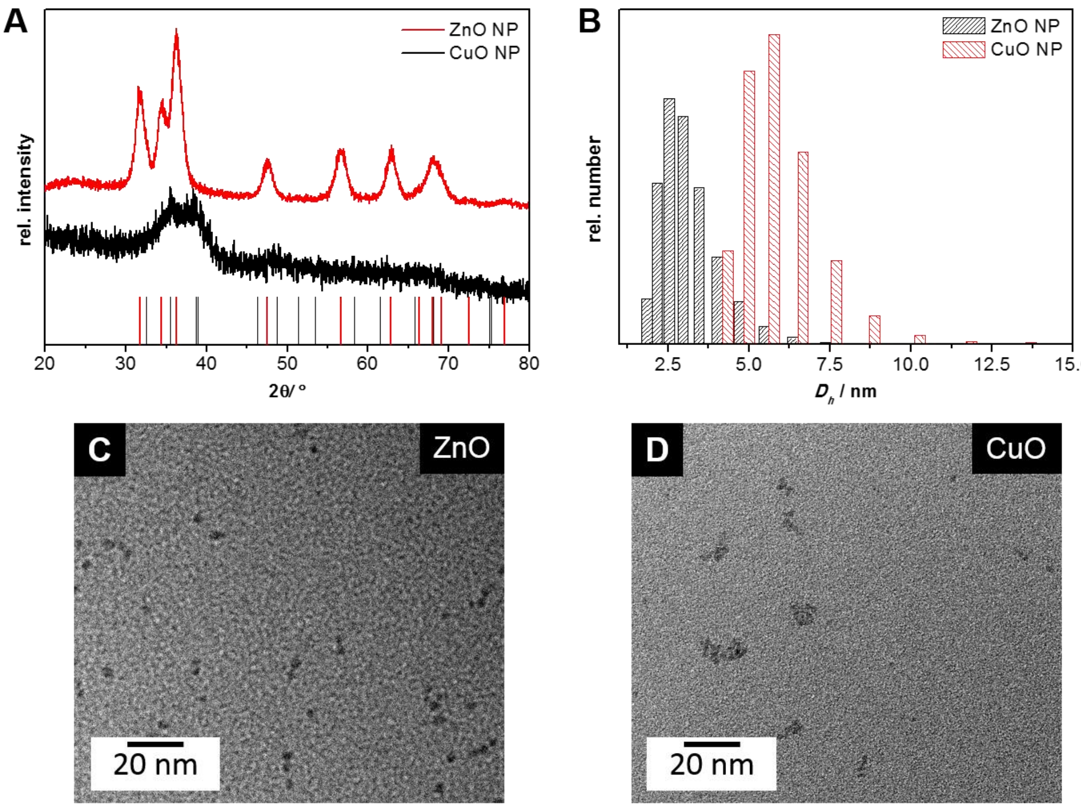

Fig. S1 PXRD pattern (A), particle size distribution obtained from DLS measurements (B) and TEM micrographs of the ZnO and CuO NPs (C, D).

2. Characterisation of citrate-stabilised Au NPs

Au NPs were synthesised according to a seeded-growth protocol by Piella et al.[2] In a first batch, citrate-stabilised seed particles (D = 4 ± 0.6 nm) were produced. In two consecutive steps, these seed particles were grown to D = 7.9 ± 0.7 nm, as revealed by TEM (Fig. S2A, B). These spherical Au NPs showed a characteristic LSPR at $\lambda_{\max}$ = 515 nm (Fig. S2C).

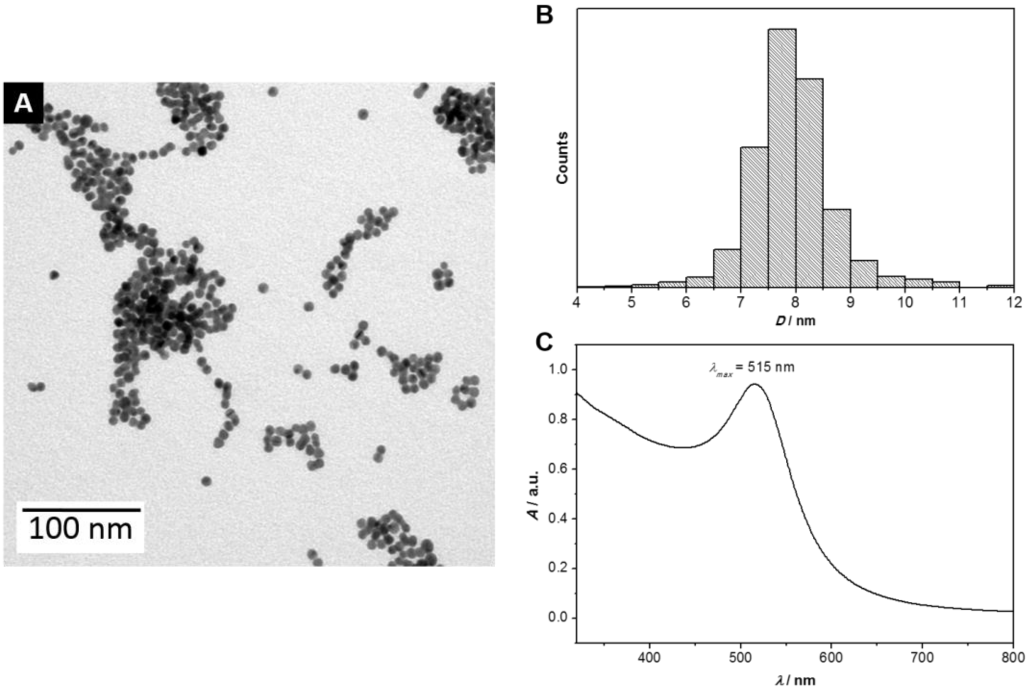

Fig. S2 TEM micrograph (A), size distribution (B) and UV-Vis spectrum ($c = 1.2 \cdot 10^{16}$ NP L^{-1} in water, (C)) of citrate-stabilised AuNPs.

3. Characterisation of trithiocarbonate-terminated PS

Trithiocarbonate-terminated PS (PS-TTC) was synthesised by reversible addition-fragmentation chain transfer (RAFT) polymerisation according to a protocol of Moad et al.[3] To this end, styrene and 2-cyano-2-propyl dodecyl trithiocarbonate (8.55 mM L^{-1}) were mixed in a ratio of 169:1. The reaction mixture was degassed for 20 min with nitrogen and subsequently heated to 110 °C for 46 h in an oil bath. The polymerisation was terminated by quenching to 0 °C with an ice bath. The product was dissolved in THF and precipitated from cold methanol.

The molecular weight of the PS-TTC was determined by THF-GPC to $M_n = 10.4$ kg mol^{-1} with a dispersity of $Đ = 1.05$ (Fig. S3A). The monomodal distribution and the low dispersity prove the controlled polymerisation of styrene. The UV-Vis spectrum shows the typical absorbance of the PS-TTC. The PS shows an absorbance maximum at about $\lambda = 250$ nm, whereas the TTC end group shows a maximum at $\lambda = 315$ nm (Fig. S3B).

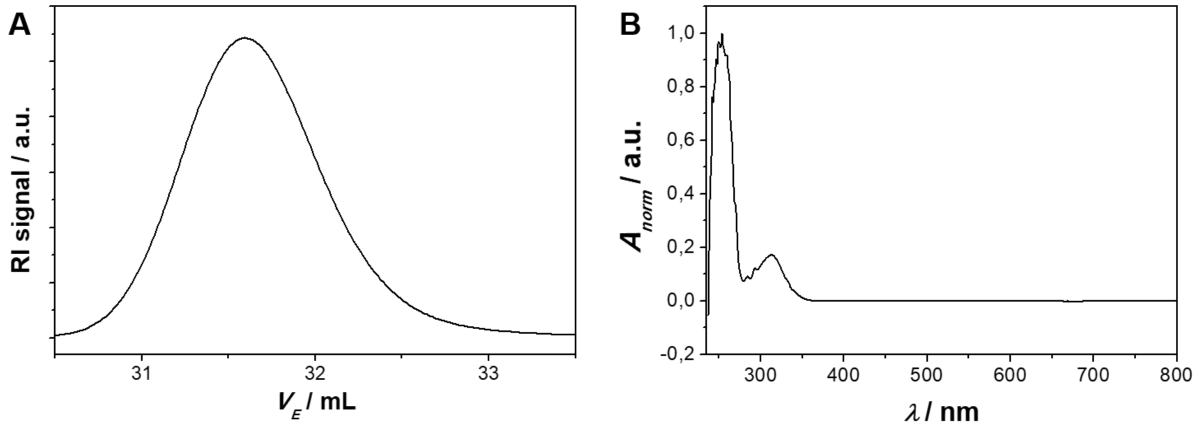

Fig. S3 THF-GPC trace (A) and UV-Vis spectrum of PS-TTC (c = 0.1 mg mL^{-1} in chloroform, (B)).

4. Characterisation of PS-stabilised Au NPs

DMF-GPC using a UV-Vis diode-array-detector was performed to show whether the PS ligands are completely bound to the Au NP surface or if free PS ligands are still present (Fig. S4A). Two different wavelengths were selected for detection, being characteristic for the PS ligand (λ = 270 nm) as well as the Au NPs (λ = 525 nm). The peak elution volume of the Au NPs is at V_E = 19 min (detection at λ = 525 nm). The corresponding GPC trace for λ = 270 nm, i.e. specific to PS, shows a bimodal distribution. The main peak at V_E = 19 min corresponds to the PS ligands bound to the Au NPs´ surface and the minor peak at V_E = 23 min to some residual free PS ligands. DLS results in an average hydrodynamic radius of R_h = 14.7 ± 0.1 nm, proving the PS shell around the Au NPs (Fig. S4B). The small standard deviation indicates the absence of agglomerates in solution.

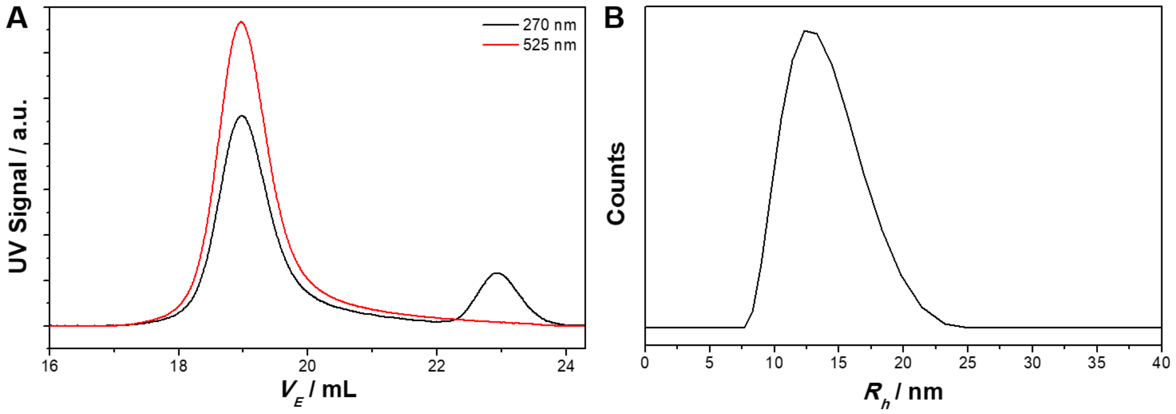

Fig. S4 DMF-GPC traces (A) and particle size distribution obtained by DLS in toluene (B) of PS@Au NPs.

5. Determination of Au NP concentration

The concentration of the PS@Au NPs in the final toluene dispersion was determined using a method reported by Hendel et al.[4] To this end, the absorbance of the PS@Au NP dispersion at λ = 400 nm before normalisation of the spectrum and the corresponding dilution factor f were used to calculate the concentration of elemental Au (equation 1).

$$[Au] = \frac{A_{400} \cdot f \cdot 1.25 \cdot 10^{-4}\, mol\, L^{-1}}{0.3} \tag{1}$$

The absorbance measured for the PS@Au NP in toluene was A_{400} = 0.5584 with a dilution factor of f = 60. To calculate the concentration of Au NPs in the dispersion, the radius of the Au NPs from TEM measurements (R_{TEM} = 4 nm), the molar mass of Au (M_{Au} = 196.97 g mol^{-1}) and the density of Au (ρ_{Au} = 19.3·10^{6} g m^{-3}) is needed. Equation 2 is used to calculate the final Au NP concentration.

$$[Au\ NP] = \frac{[Au] \cdot M_{Au}}{\frac{4}{3} \cdot R_{TEM}^{3} \cdot \pi \cdot \rho_{Au}} \tag{2}$$

This yields in an Au NP concentration of [Au NP] = 5.3·10^{17} NP L^{-1}.

6. Characterisation of the amidated PMMA homopolymer

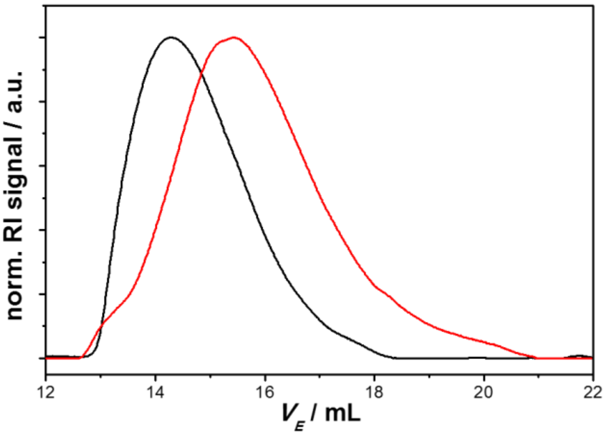

Fig. S5 HFIP-GPC traces of PMMA (red) and amidated PMMA (black).

7. Characterisation of the *s*-SEDMA triblock terpolymer

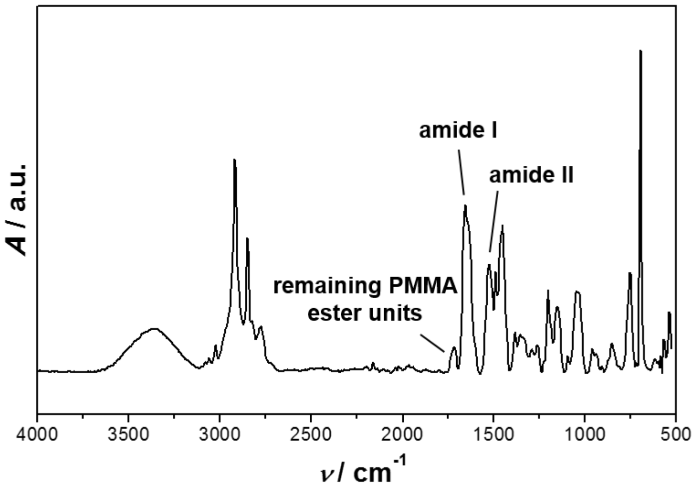

Fig. S6 FT-IR spectrum of *s*-SEDMA.

8. Characterisation of *as*-SEDMA

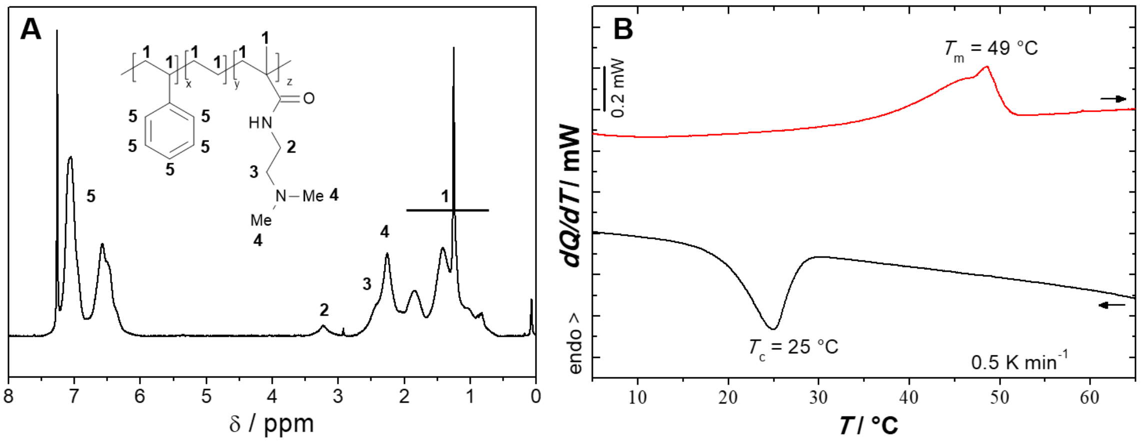

Fig. S7 ^{1}H-NMR spectrum measured in $CDCl_3$ (A) and µDSC heating and cooling traces (c = 10 g L^{-1} in THF, (B)) of *as*-SEDMA.

9. Optical properties of the *as*-SEDMA hybrid micelles

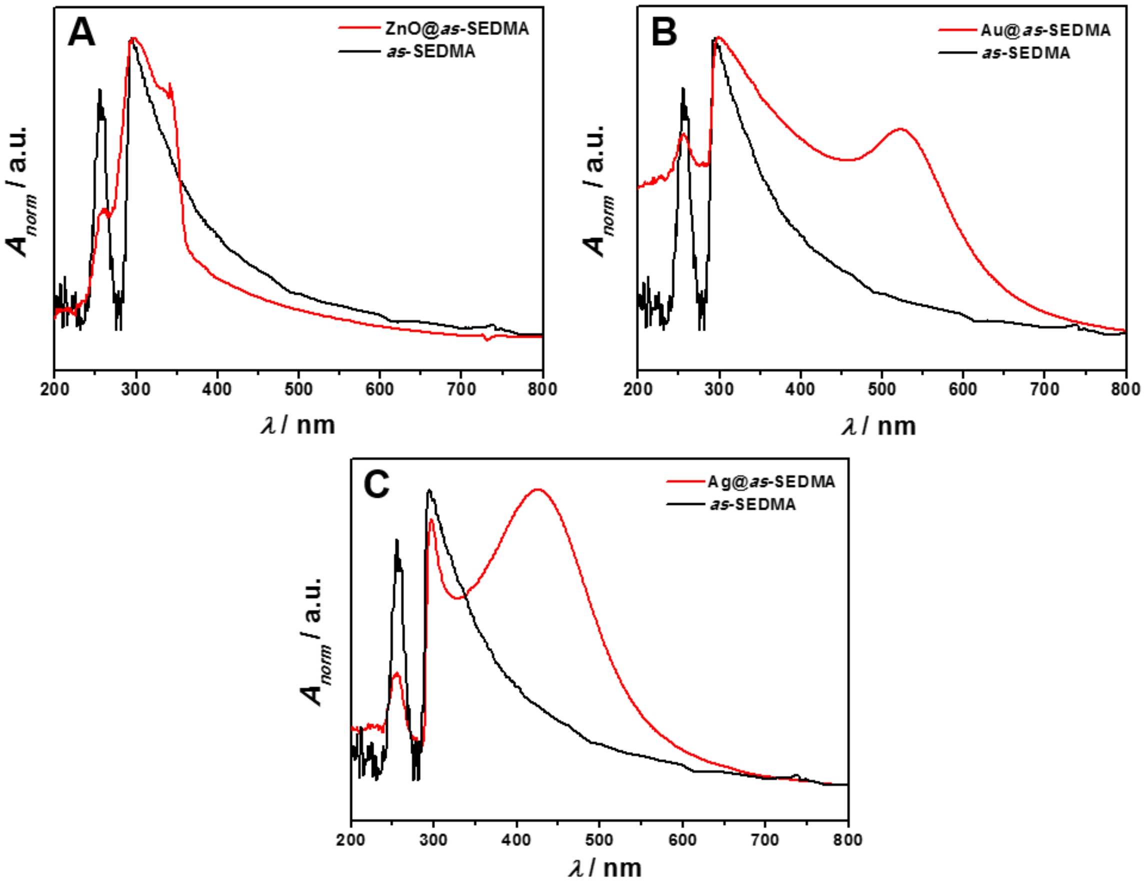

Fig. S8 UV-Vis spectra of *as*-SEDMA hybrid micelles with ZnO (A), Au (B) and Ag (C) NPs.

10. ZnO/*as*-SEDMA hybrid wCCMs in acetone

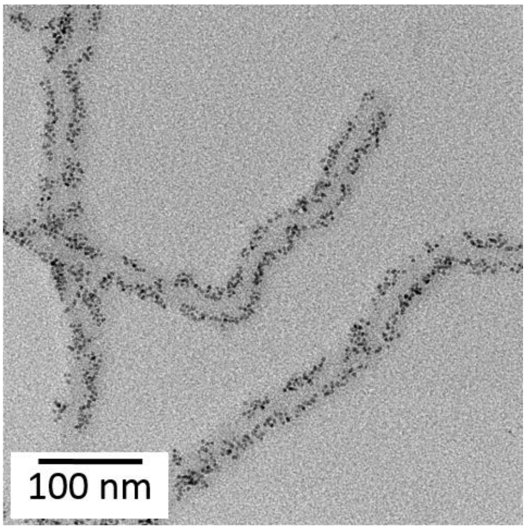

Fig. S9 TEM micrograph of *as*-SEDMA/ZnO NP hybrid wCCMs (dispersion in THF/acetone = 10/90 (v/v)).

11. *In situ* synthesis of Ag NPs in the presence of non-functionalized $S_{48}E_{27}M_{25}^{141}$ wCCMs

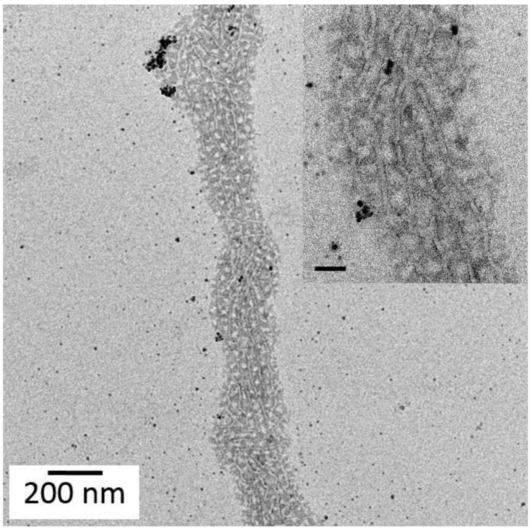

Fig. S10 Blend of Ag NPs and $S_{48}E_{27}M_{25}^{141}$ wCCMs. The absence of functional groups for the incorporation of Ag NPs in the wCCM corona leads to a statistical distribution of free Ag NPs and several agglomerates over the whole copper grid. The scale bar in the inset corresponds to 50 nm.

12. Continuous loading by microfluidics

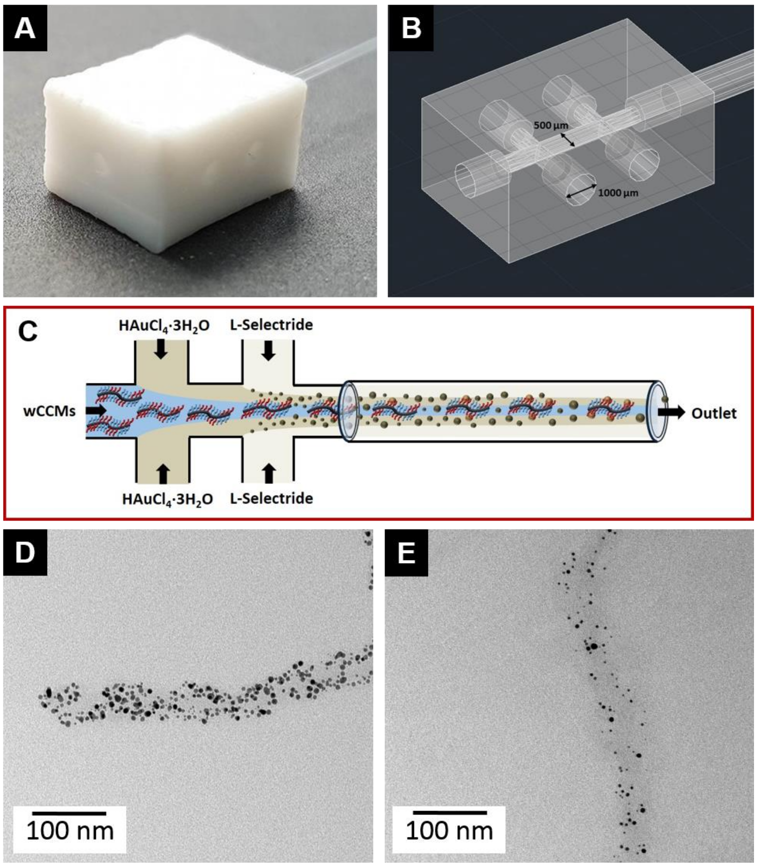

Fig. S11 For optimum mixing of the educts, we fabricated an individually designed microfluidic device based on a home-made PTFE chip (A) with a double-focusing cross that is made of four side channels and finally connected to a glass capillary (inner diameter D = 980 µm) *via* the central main channel, as visible in the detailed CAD-design (B). Illustration of the fluid focusing within the tailor-made microfluidic device (C). TEM micrograph (D) of the *s*-SEDMA/Au hybrid micelles prepared at following flow rates: *s*-SEDMA wCCMs: 2000 µL h^{-1}, $HAuCl_4 \cdot 3H_2O$: 2000 µL h^{-1} and L-Selectride: 1000 µL h^{-1} ($Q = 8000$ µL/h, $t = 17.0$ s). Reducing the flow rate of $HAuCl_4 \cdot 3H_2O$ by half, while keeping the other flow rates constant ($Q = 6000$ µL/h, $t = 22.6$ s), results in a decreased loading of the wCCMs with Au NPs as revealed by TEM (E). The diameter of the Au NPs (D = 3.4 ± 1.6 nm) is slightly reduced in comparison to the highly loaded *s*-SEDMA wCCMs prepared at a higher flow rate of the metal precursor (D = 4.3 ± 1.4 nm).

13. Aggregation behaviour of PS@Au NPs

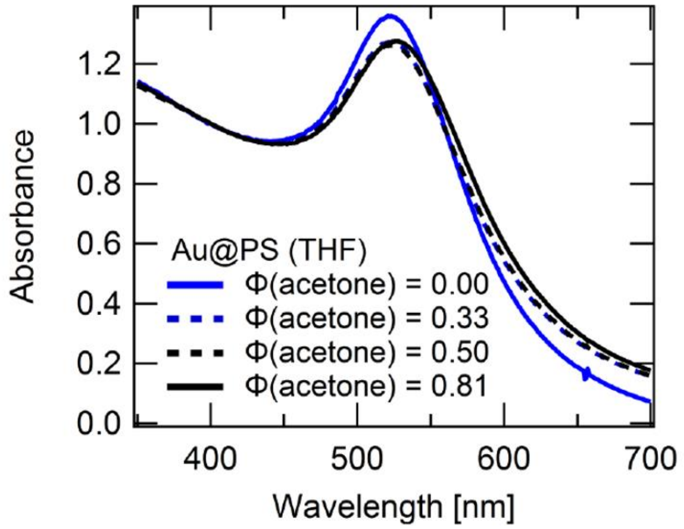

Fig. S12 UV-Vis spectra of PS@Au NPs in different solvent mixtures of THF and acetone.

14. ZnO/*s*-SEDMA hybrid wCCMs in acetone

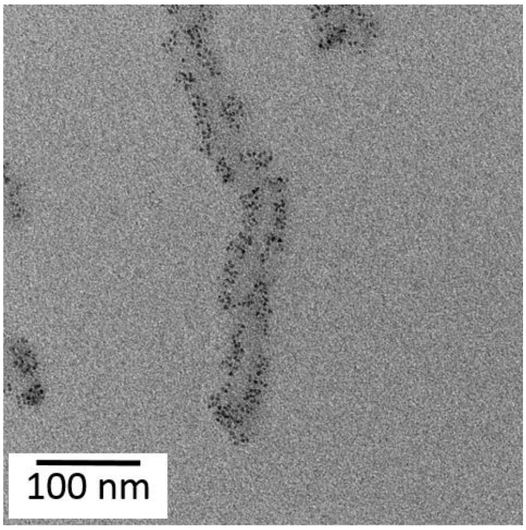

Fig. S13 TEM micrograph of the *s*-SEDMA/ZnO NP hybrid wCCMs (dispersion in THF/acetone 10/90 (v/v)).

15. Binary loading of *s*-SEDMA wCCMs with Ag and PS@Au NPs

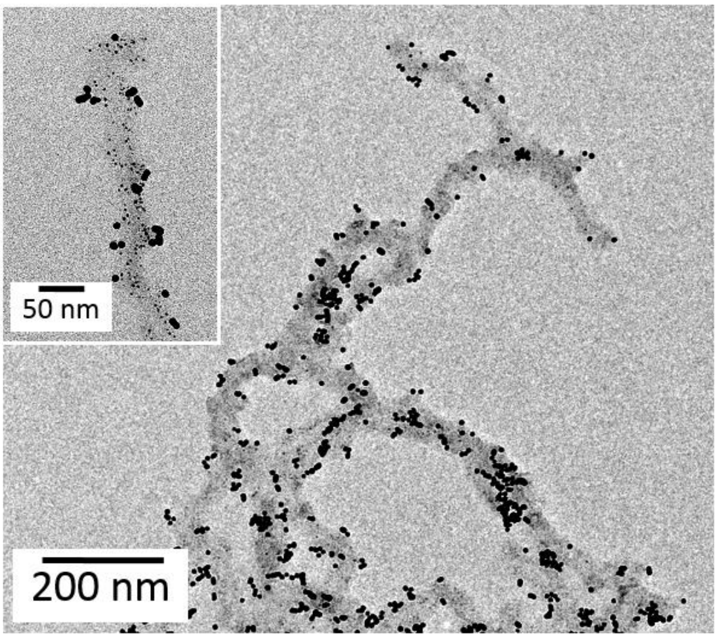

Fig. S14 TEM micrograph of binary loaded *s*-SEDMA wCCMs with Ag and PS@Au NPs.

16. References

1 T. Kida, T. Oka, M. Nagano, Y. Ishiwata and X. G. Zheng, *J. Am. Ceram. Soc.*, 2007, **90**, 107–110.

2 J. Piella, N. G. Bastús and V. Puntes, *Chem. Mater.*, 2016, **28**, 1066–1075.

3 G. Moad, J. Chiefari, Y. K. Chong, J. Krstina, R. T. A. Mayadunne, A. Postma, E. Rizzardo and S. H. Thang, *Polym. Int.*, 2000, **49**, 993–1001.

4 T. Hendel, M. Wuithschick, F. Kettemann, A. Birnbaum, K. Rademann and J. Polte, *Anal. Chem.*, 2014, **86**, 11115–11124.